SSRG International Journal of Electronics and Communication Engineering
ISSN: 2348-8549/ https://doi.org/10.14445/23488549/IJECE-V13I6P112

Volume 13 Issue 6, 145-153, June 2026
© 2026 Seventh Sense Research Group®

Original Article

An Investigation on Performance Enhancement of GaAs Solar Cells Using an $Al_{0.41}Ga_{0.59}As$ Window Layer

Jhilirani Nayak[1], Pankaj Prusty[1*], Priyabrata Pattanaik[1], Dilip Kumar Mishra[1]

[1]*Faculty of Engineering and Technology (FET), Siksha 'O' Anusandhan Deemed to be University, Bhubaneswar, India.*

[*]*Corresponding Author : pankajprusty@soa.ac.in*

Received: 13 March 2026 Revised: 12 April 2026 Accepted: 11 May 2026 Published: 27 June 2026

Abstract *- Gallium Arsenide (GaAs) single-junction solar cells lead in advanced photovoltaic research due to its high absorption coefficients, favourable high bandgap, and strong potential for high conversion efficiency. This paper presents numerical simulation and performance optimization of an AlGaAs window layer-based heterojunction solar cell incorporated with $Al_{0.41}Ga_{0.59}As$ front passivation layer, n+- GaAs carrier injection layer, a p-GaAs absorber layer, a p-$Al_{0.41}Ga_{0.59}As$ Back Surface Field (BSF) layer, and a p+-GaAs interface layer. The aluminum composition of 41% is selected in order to achieve optimal band alignment and reduced recombination losses. The wide-bandgap AlGaAs layers are used at the front and rear interfaces in order to enhance carrier collection, zero-bias current density, and no-load voltage. The n^{++}/p polarity exhibits higher electron mobility, results in a simulated zero-bias current density of 31.36mA/cm^2,1.31V of no-load voltage, and a output power quality factor of 83.31%. The optimized device achieves a peak photovoltaic conversion efficiency of 34.38% under 1.5G illumination.*

Keywords *- High-Efficient Photovoltaic Cell, SCAPS, AlGaAs Window Layer, n^+/p Cell, Back Surface Field Layer.*

1. Introduction

The global energy is rapidly growing towards renewable sources. Among renewable options, Photovoltaic (PV) technology has attracted substantial interest, as it can convert sunlight directly into electricity with minimal emissions [1], [2]. Silicon-based PV modules are currently dominating the photovoltaic industry. However, it needs improvement in material systems and device architectures to reach higher Power Conversion Efficiencies (PCE), while reducing material consumption and production costs [1, 3]. This pursuit led to increase research on compound semiconductor materials, particularly III–V systems, which exhibit superior optoelectronic properties compared to silicon [4, 5].

Gallium Arsenide (GaAs) represents a primary material in III–V photovoltaics as it has a direct bandgap of approximately 1.42 eV, high absorption coefficient, and advantageous carrier transport characteristics [5]. The intrinsic parameters enable efficient photon absorption, reduce bulk recombination losses, and support high currents [6]. GaAs solar cells have achieved an efficiency of more than 27 % in laboratories, especially under advanced epitaxial growth processes and heterojunction engineering. GaAs demonstrates significant temperature robustness and radiation hardness. Due to which GaAs photovoltaic cells are ideal for space applications and high-Concentration Photovoltaic (CPV) Systems [7, 8]. Its performance is limited due to surface and interface recombination. Photogenerated carriers recombine non-radiatively near the illuminated surface before contributing to photocurrent. Hence, it reduces the current density (J_{sc}) and open-circuit voltage (V_{ov}) [9]. According to the device design, a thinner absorber layer reduces material use and fabrication complexity. As a result, the effect of surface recombination becomes more significant, demanding the advanced surface passivation and optical management strategies [10, 11]. A method to reduce the effect of surface losses involves integration of a wide-bandgap window layer onto the front surface of the cell.

This layer behaves as a passivation and optical transmission interface. It allows high-energy photons to reach the absorber layer while suppressing recombination at the surface [12, 13]. Aluminum Gallium Arsenide (AlGaAs) is the most effective window layer material for GaAs solar cells, based on its excellent lattice matching, tunable bandgap, and electronic properties [13, 14]. By adjusting the aluminum composition, the bandgap of $Al_xGa_{1-x}As$ can be adjusted to reduce parasitic absorption and enhance photon delivery to the beneath layers [14, 15].

AlGaAs/GaAs heterojunction provides proper band alignment that improves charge separation and carrier confinement. It also decreases surface recombination velocity and enhances V_{oc} and J_{sc} [14]. The optimization of window layer thickness and doping profile enhances fill factor and conversion efficiency. The incorporation of AlGaAs window

This is an open access article under the CC BY-NC-ND license (http://creativecommons.org/licenses/by-nc-nd/4.0/)

layer enhances optical properties like antireflection coatings and light-trapping nanostructures, and boosts the device performance [16].

The recent research includes dielectric composite nanostructures that reduce surface reflectance and increase absorption across the solar spectrum. These structures exploit resonant effects to trap light within the absorber while minimizing losses. The optimized composition and thickness of the AlGaAs layer provide enhanced performance, while excessive Aluminium content introduces defects, oxidation, and higher resistances.

The insufficient bandgap may not effectively supress recombination. So, the systematic investigation of window layer parameters are essential to maximize the device efficiency without compromising electrical stability. The integration of AlGaAs window layer into heterojunctions like graphene/ AlGaAs/GaAs Schottky cells with surface texturing has resulted in better efficiency due to reduced optical losses and improved charge collection [4].

The present work analyzes the behaviour of the designed solar structure in the presence of an AlGaAs window layer. It examines the influence of window layer properties on photovoltaic parameters of the n+/p GaAs photovoltaic cell. The results are expected to contribute to the ongoing development of GaAs solar cells.

The n+/p polarity configuration has provided superior efficiency when compared to previously documented solar cell performances. The study explains that the AlGaAs interface layer helps to minimize surface recombination by introducing a larger bandgap barrier at the emitter interface. This barrier reduces minority carrier losses and enhances carrier confinement.

2. Materials and Methods

The SCAPS simulation tool was used to simulate the Gallium Arsenide solar structure. This is a specialized one-dimensional program designed for the analysis of heterojunction photovoltaic devices. This software allows for a detailed exploration of the electrical and optical properties of the structured device.

Key components of the simulation tool include the formulation and solution of one-dimensional semiconductor equations. These equations together provide the basis for simulating and analyzing how the device behaves [17].

$$\frac{\partial}{\partial x}\left(\varepsilon_0 \varepsilon \frac{\partial \psi}{\partial x}\right) = -q\left(p - n + N_D^+ - N_A^- + \frac{\rho_{def}}{q}\right) \quad (1)$$

$$-\frac{\partial J_n}{\partial x} - U_n + G = \frac{\partial n}{\partial t} \quad (2)$$

$$-\frac{\partial J_p}{\partial x} - U_p + G = \frac{\partial p}{\partial t} \quad (3)$$

$$J_n = -\frac{\mu_n n}{q}\frac{\partial E_{Fn}}{\partial x} \quad (4)$$

$$J_p = +\frac{\mu_p p}{q}\frac{\partial E_{Fp}}{\partial x} \quad (5)$$

Where the key parameters and their units with SCAPS simulation ranges are denoted in the below Table 1. In the presented framework, various key parameters are defined: ε represents the permittivity, ρ characterizes the space charge density, ψ denotes the electrostatic field potential relative to the vacuum energy level, J_n and J_p stands for carrier transport current density, G and U signifies the optical generation rate and net concentration rate, while $\frac{\partial n}{\partial t}$ and $\frac{\partial p}{\partial t}$ indicate the rates of change in electron and hole concentrations.

Recombination rates within the cells have been computed employing the Shockley- Read-Hall recombination model. The SCAPS 1D tool is a powerful simulation tool. It is used to simulate 1D planar structures instead of 3D real-world devices. Non-uniform illumination, edge effects, and series resistance effects cannot be analysed using SCAPS. It is not applicable for a texture simulation. In spite of all this, it is an excellent tool for quick simulation and prototyping.

The SCAPS simulation tool has been employed to compute both the steady-state and small-signal solutions of the proposed system. Small-signal analysis has been conducted to derive the system's conductance and capacitance. Four distinct measurements, namely I-V curve(current-voltage curve), C-V curve (capacitance versus voltage curve), C-F curve (capacitance versus frequency curve), and Q-E curve(charge-extraction curve), have been conducted using this simulation tool. The numerical solution of the bulk layer Equations (1), (2), and (3) was achieved through Gummel's iteration scheme in conjunction with the sub-steps of the Newton-Raphson method.

The following steps outline the process for obtaining a solution. The device parameter calculation begins at the starting point and then gradually moves toward the equilibrium state. At this point, there is no external light or voltage applied. The device was operated in darkness. The equilibrium state served as the starting point to calculate the device's performance in working conditions.

Then, illumination was introduced to obtain the short-circuit condition. It was used as the new starting point for calculation. Gradually, the applied bias voltage was increased, and the operating point was calculated. After this, the initial data point was computed to simulate the measurement process [17]. For the I-V curve, a voltage range that was independent of the working point voltage was given. The required parameters are listed below to simulate the proposed cell.

Table 1. Material parameters for GaAs/AlGaAs-based solar cell layers in SCAPS simulations

Parameters	p^+- GaAs(Buffer)	AlGaAs(BSF)	p-GaAs	n-GaAs	AlGaAs (Window layer)
Thickness(µm)	0.5	0.5	2.0	0.1	0.02
Dielectric Constant	4.07	3.740	4.07	4.07	3.740
Electron affinity(eV)	12.9	10.6	12.9	12.9	10.6
Forbidden energy gap(eV)	1.424	1.973	1.424	1.424	1.973
Conduction band carrier state density(cm^{-3})	1x 10^{17}	8x 10^{19}	1x 10^{17}	1x 10^{17}	8x 10^{19}
Valence band carrier state density(cm^{-3})	1x 10^{19}	1x 10^{19}	1x 10^{19}	1x 10^{19}	1x 10^{19}
Effective electron mobility (cm^2 /Vs)	8500	212	8500	8500	212
Effective hole mobility (cm^2 /Vs)	370	126	370	370	126
Concentration of acceptor dopants (cm^{-3})	1x10^{18}	1x10^{17}	1x10^{16}	0	0
Concentration of donor dopants (cm^{-3})	0	0	0	2 x10^{19}	2 x10^{19}
Electron thermal velocity (cm/s)	4.4x 10^5	2.3x 10^5	4.4x 10^5	4.4x 10^5	2.3x 10^5
Hole thermal velocity (cm/s)	1x10^5	1.4x10^5	1x10^5	1x10^5	1.4x10^5

3. Model Calibration and Feasibility of Fabrication

This section presents the calibration of the device by comparing its characteristics with the previously reported characteristics [18]. The fabrication process of GaAs buffer layers were done by growing them using Molecular Beam Epitaxy(MBE) and then subjected to thermal cycle annealing [19]. To fabricate GaAs solar cells, photolithography and deposition of metal contacts on the front surface were done [18]. The output calibration were done by comparison with the early reported reference [18]. Figure 1 illustrates the J-V response curve of the present structure. It closely follows the trend observed in the plot of reference [18]. In the reference study [18], the fabricated device featured 0.122 cm^2 of active area, resulting in an efficiency of 16.8%. The trade-off in the curve of Figure 1 occurs at 1.02V. Current density reaches zero value at a voltage of approximately 1.3V. The proposed device provides an efficiency of 34.38% featured of an effective area of 1cm^2. The trade-off in the curve of Figure 1 occurs at 1.02V. Current density attains a zero value at a voltage of approximately 1.31V.

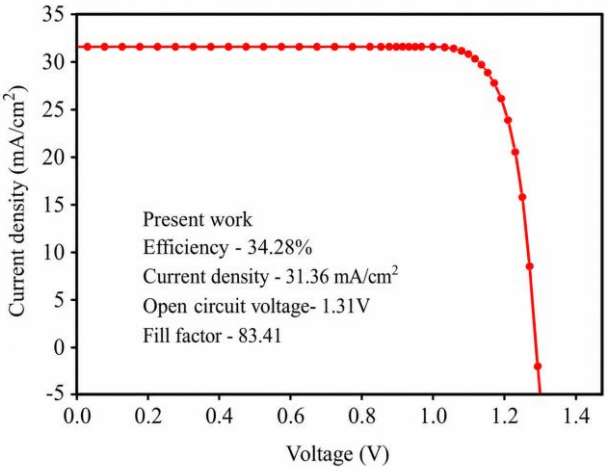

Fig. 1 Represents electrical performance of the simulated solar cell

4. Results and Discussion

A comprehensive simulation study was conducted for the proposed device to describe its key parameters. The device comprises the following layers: a front contact, an AlGaAs window layer, a GaAs-based emitter and base layers, an AlGaAs Back Surface Field (BSF) layer, a GaAs interfacial layer, and a back conductive layer. The simulation was performed using specified material parameters detailed in Table 1, encompassing various electrical properties. Figure 2(a) visually represents the architectural structure of the solar cell, while Figure 2(b) illustrates the spectrum employed for illuminating the cell. Subsequently, Figures 3(a) and (b) present the characteristic curve of the device, providing insights into its performance characteristics.

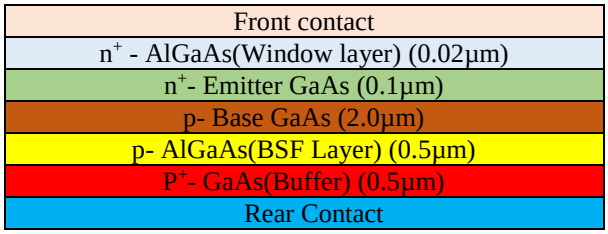

(a)

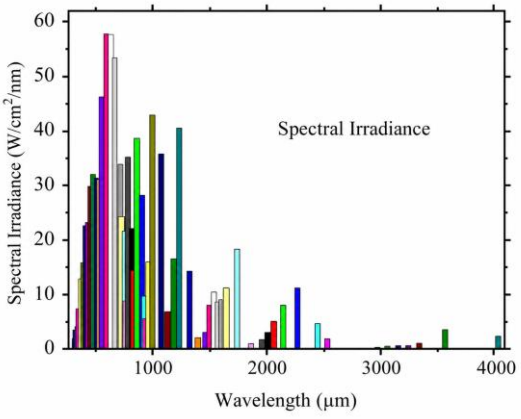

(b)

Fig. 2 (a) A structural model of the five-layered GaAs solar cell and (b) The spectrum used to illuminate the cell

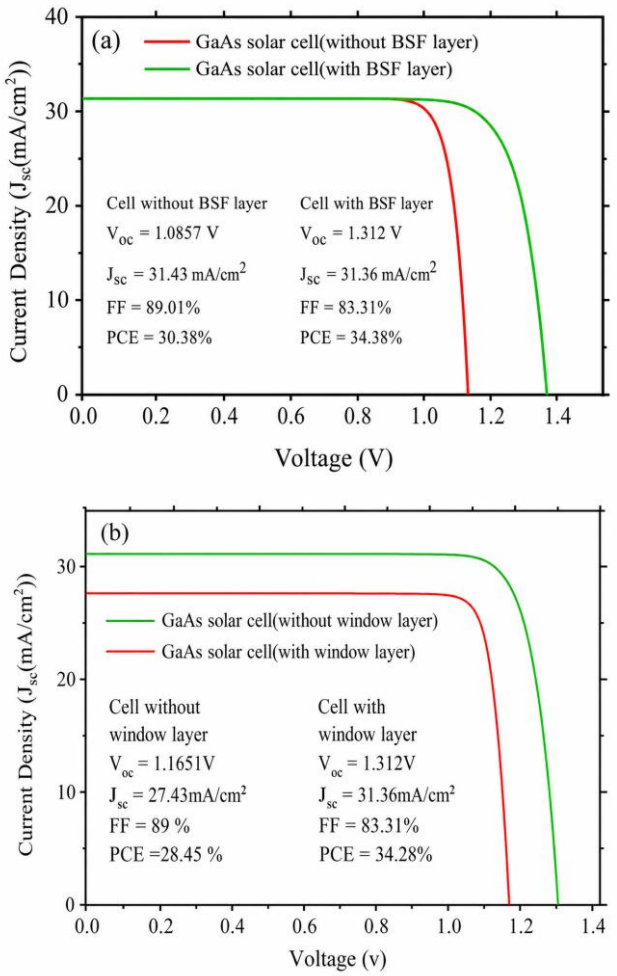

Fig. 3 Represents J-V performance analysis of GaAs solar cell (a) With and without rear surface field layer, and (b) With and without window layer.

Figure 3(b) provides a graphical representation of the characteristics curve with and without the window layer. The $Al_{0.41}Ga_{0.59}As$ top interface layer acts as a good transparent and passivating layer. It provides interfacial tunneling due to band offset and thin-layer effects. The minimization of recombination loss and effective collection of high-energy carriers leads to higher current output and better overall efficiency. In the presence of the wide bandgap AlGaAs window layer, the photovoltaic cell exhibits notable performance metrics, including a 34.38% efficiency, V_{oc} of 1.31 V, J_{sc} of 31.36 mA/cm^2, and a fill factor of 83.31%. These values have been achieved at a window layer thickness of 0.02µm at a doping level density of 1×10^{17} atoms/cm^3, emitting layer width of 0.8µm at a concentration of 2×10^{19} atoms/cm^3, base layer thickness of 2.0µm at 1×10^{16} atoms/cm^3 and back surface layer thickness of 0.5µm at 1×10^{17} atoms/cm^3. However, integration of the AlGaAs BSF layer results in a marginal efficiency improvement, as shown in Figure 3(b), elevating efficiency from 30.38% to 34.38%. It is observed that the FF experiences a reduction from 89% to 83.31%. The fill factor reduction in the BSF layer is due to its thickness. The device is designed with a BSF layer thickness of 0.5µm. This is sufficient to create an electric field that repels minority carriers, as a result increases the cumulative resistive component. The increased resistance and the doping of the material reduce the fill factor. This observation underscores the substantial role played by the back-surface field layer in enhancing efficiency, primarily by mitigating recombination events at the surface. This reduction in recombination stems from the induced electric field, which effectively repels electrons towards the junction interface. Figure 4 illustrates the band diagram of the heterojunction device. At the junction interface, the intra-band tunneling effect is created due to a high electric field, which is a result of high doping concentration. The presence of the tunneling effect shown in Figure 4 increases the recombination of carriers, which limits the zero-voltage operating current.

Figure 5: The energy band diagram represents the formation of an electric field. Figure 3(b) provides a comparative visualization of the photovoltaic cell with and without the window layer. The improvements were made to the structured photovoltaic cell by optimizing the doping concentration of both the window and BSF layers, as well as adjusting the thickness of those layers. Figure 6 illustrates the variations of different cell characteristics with respect to the thickness of the emitter layer. In Figure 6(d), it becomes evident that the conversion efficiency is high at a bandgap of 1.2eV. eV. This is due to the optimization conflict between optical absorption and carrier thermalization losses.

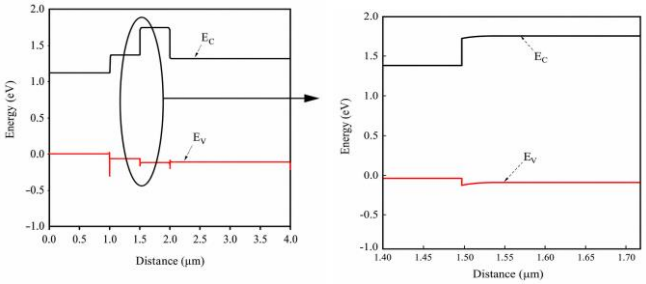

Fig. 4 Energy band diagram of the proposed solar cell

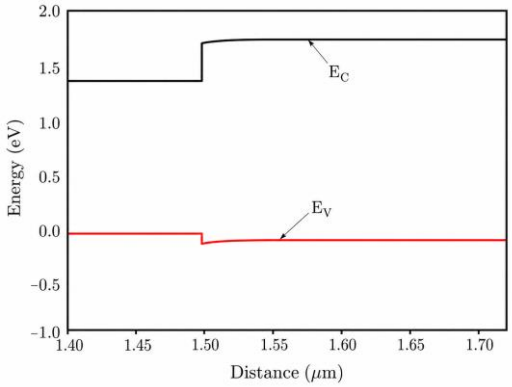

Fig. 5 Formation of the back-surface field

The open-circuit voltage begins to saturate within the bandgap range of 1.3 eV to 1.42eV, irrespective of any further increase in thickness, as shown in Figure 6(a). Furthermore, beyond a bandgap of 1.4 eV, the fill factor also exhibits a saturation trend shown in Figure 6(c). This saturation effect is due to the diminished photovoltaic response at elevated bandgap values. This is due to a significant portion of electrons fails to contribute to the photovoltaic effect. It is observed that the voltage experiences a decline at a specific bandgap. This happens primarily due to the reduced internal electric field and increasing emitter thickness. The current density follows the same trend as efficiency in Figure 6(b). Figure 7 provides a comprehensive depiction of various cell parameters as functions of both bandgap and distinct base thickness values. These parameters exhibit variations with different base thicknesses and bandgap values. Notably, the cell efficiency demonstrates an increase up to a base thickness of 2 µm, followed by a subsequent decrease beyond this threshold.

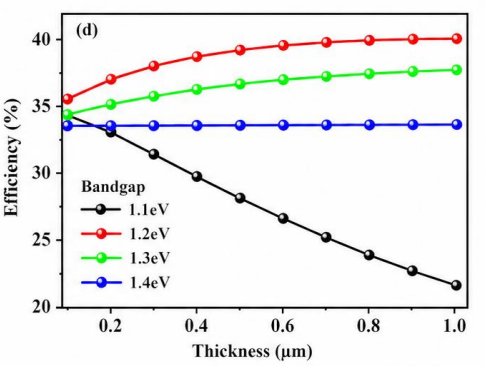

Fig. 6 Figure illustrates the parameters in relation to the varying width of the emitter section corresponding to different band gaps. (a) Open circuit voltage, (b) Short circuit current density,(c) Fill factor, and (d) Efficiency

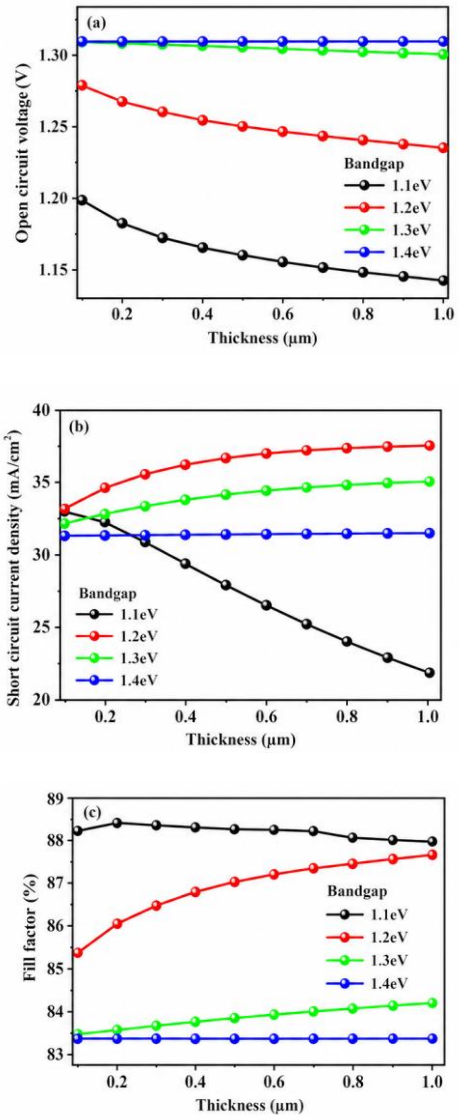

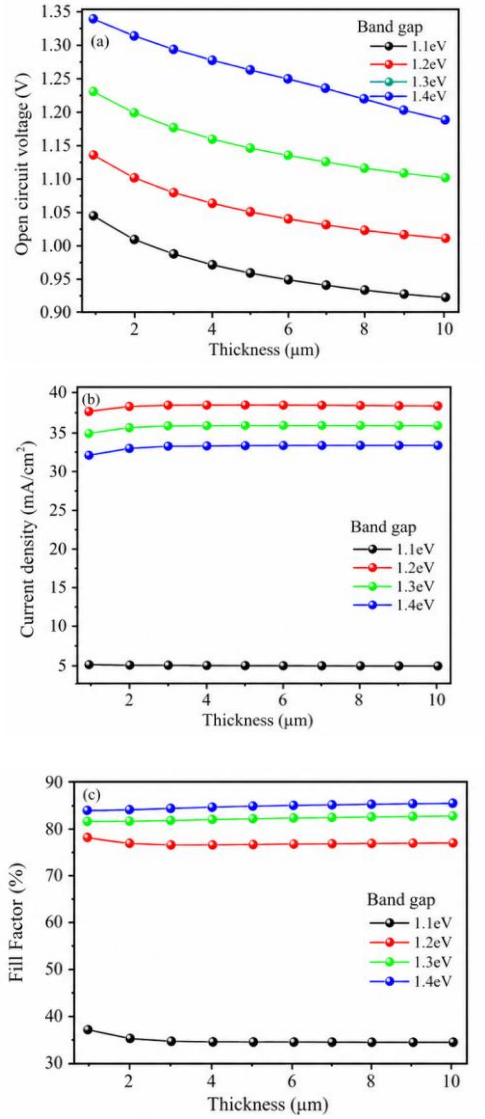

Fig. 7 Figure represents the electrical parameters of GaAs solar cells according to varying base thickness corresponding to different band gaps. (a) Open circuit voltage, (b) Short circuit current density, (c) Fill factor, and (d) Efficiency

Figure 7 shows variations of electrical parameters with respect to a rise in base thickness. Each curve represents a variation with respect to a bandgap. Figure 7(a) illustrates the decaying of the voltage with a rise in thickness. It exhibits a fall within the range of 1µm to 10µm. This phenomenon is due to the built-in field effect across the junction as the base thickness increases. The base layer is a critical structure to influence the optoelectronic performance of the device. In this work, increasing base thickness leads to a monotonic rise in J_{sc}. Figure 7(b) highlights that the peak value of J_{sc} is at a bandgap of 1.2 eV, where the base thickness is 5µm. This monotonic behavior is due to efficient utilization of incident photons within the base region. The simulation further reveals that an increase in base thickness leads to enhanced bulk recombination, which saturates J_{sc}. Figure 7(c) demonstrates the reduction of the fill factor. The electrical simulation results with a higher resistance due to increase base thickness. As a result of which, the carrier transport path rises, and ultimately the fill Factor reduces. Figure 7(d) exhibits the efficiency curve. The conversion efficiency rises to its maximum value at a base thickness of 1µm. Then, it subsequently decreases due to recombination and resistive losses. Figure 8 presents the variations of key electrical parameters with respect to emitter doping concentration. The Figure 8(a) indicates that the open-circuit voltage saturates beyond a threshold concentration of 5×10^{18} atoms/cm^3. The current density curves in Figure 8(b) attain a saturation level at a concentration of 1×10^{17} atoms/cm^3, and the fill factor in Figure 8(c) reaches its zenith at a concentration of 1×10^{17} atoms/cm^3, subsequently declining for higher concentrations. The efficiency curves in Figure 8(d) show an initial increase and then remain constant. An optimal efficiency of 34.38% is achieved at a thickness of 0.5µm and a concentration of 5×10^{17} atoms/cm^3.

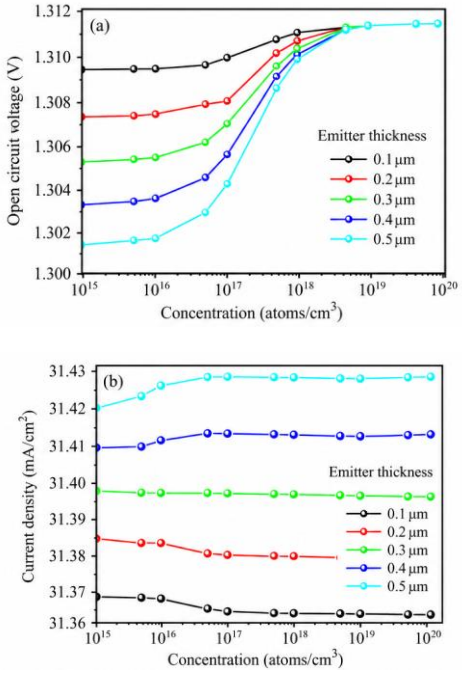

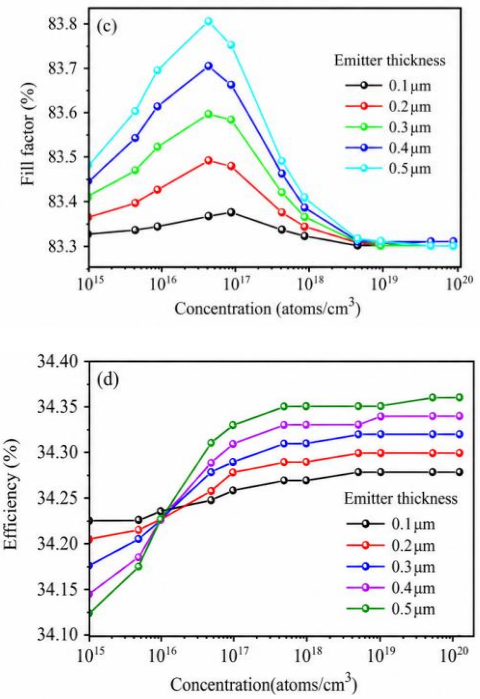

Fig. 8 Estimated electrical parameters of the simulated GaAs photovoltaic cell in relation to emitter concentration

Figure 9 describes the responses with respect to variations in the thickness of the rear surface field layer. In Figure 9(a), the curve rises from 1.309 V to 1.313 V, indicating that with a rise in doping concentration, the open circuit voltage rises. Figure 9(c) and (d) exhibit an upward trend followed by saturation as the doping concentration increases. Along with this, the current density in Figure 9 (b) shows only marginal alterations with the changing doping concentration. These observed changes are due to the internal electric field.

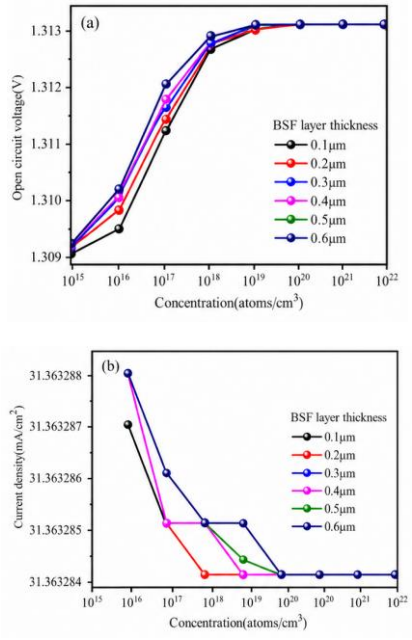

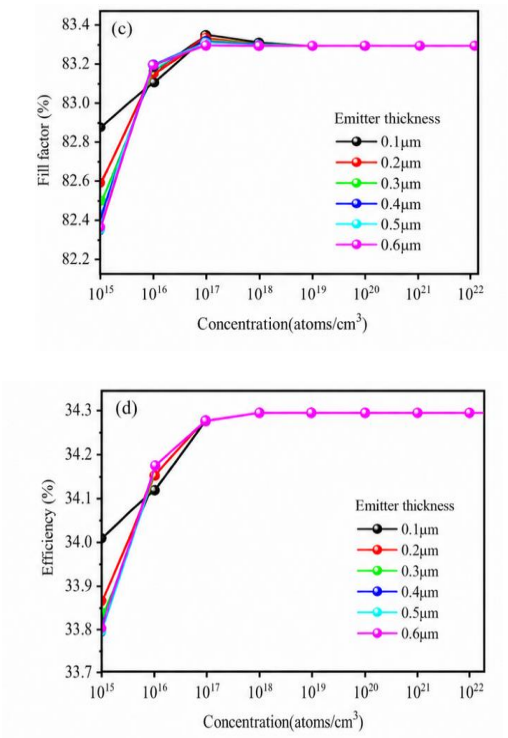

Fig. 9 Estimated electrical parameters of the simulated GaAs photovoltaic cell as a function of rear surface field layer concentration.

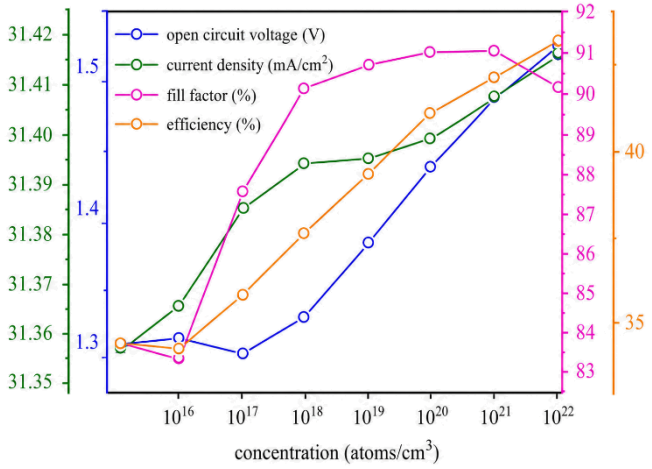

Fig. 10 Estimated electrical parameters of the simulated photovoltaic cell as a function of buffer layer concentration corresponding to a thickness of 2.0μm

Figure 10 provides the responses of the proposed device at a buffer layer thickness of 2.0μm. There is a rise in the value of all parameters with a rise in concentration. The increase in efficiency and current is due to a larger number of available charge carriers. Figure 11(a) and (b) present the impact of temperature on critical electrical parameters. The rise in temperature increases the no-load voltage as shown in Figure 11 (a).

This response is due to a substantial rise in the saturation current under reverse bias. The changes in zero-bias current are less in comparison to voltage, but it cannot compensate for the loss in open circuit voltage. Figure 11(b) shows the decrease in fill factor with an increase in temperature. This decrease response is primarily due to the enhanced recombination losses and increased carrier scattering. The combine effect of voltage, current, and fill Factor reduces the conversion efficiency as shown in Figure 11(b).

Table 2 offers a comparison between the results of the designed structure and previously reported research. The present work exhibits exceptional efficiency due to high zero-bias current density (J_{sc}). The Gallium arsenide solar device provides a relatively lower output power quality factor and a remarkable high no-load voltage.

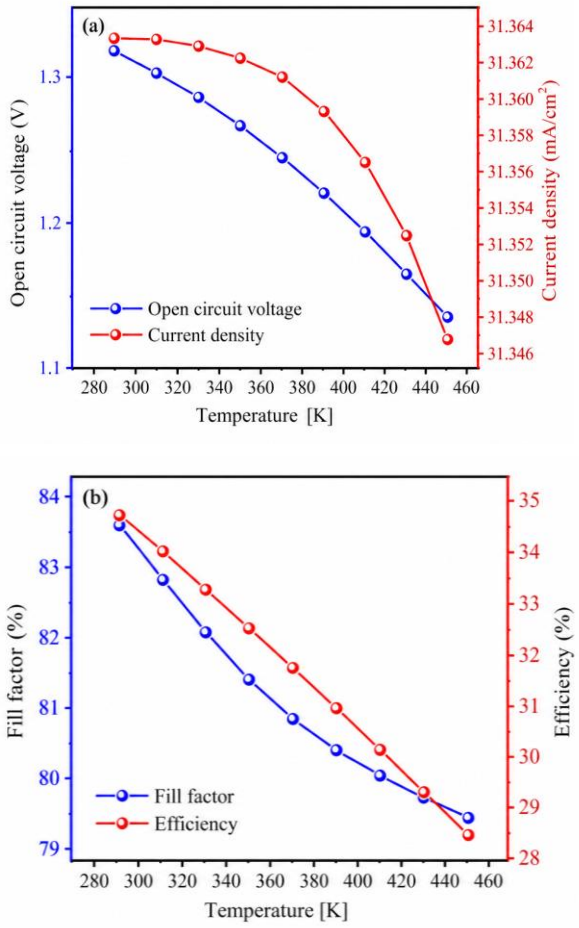

Fig. 11 Influence of temperature on (a) No-load voltage and current density and (b) Fill factor and efficiency

Table 2. Model validation

Solar Cell Model	Spectrum	No-load Voltage(V_{oc})	Zero-bias Current Density (J_{sc})	Fill Factor(FF)	Conversion Efficiency(η)
Shizhao et al. [18]	AM1.5G	0.8545V	26.45mA/cm^2	74.25%	16.78%
Duy phong Pham et al.[20](Expt.)	AM1.5G	0.973V	27.75mA/cm^2	83.9%	22.65%
Duy phong Pham et al.[20](Simulation)	AM1.5G	0.970V	27.78mA/cm^2	83.99%	22.63%
Knechtli et al.[21] (Experimental)	AM0	1.02V	119.8mA/cm^2	84%	19.0%
Knechtli et al.[21] (Theory)	AM0	1.02V	116.1mA/cm^2	85%	18.5%
Z. Ren et al.[22]	AM1.5G	2.08V	11.3mA/cm^2	76%	17.8%
S.-T.Hwang et al.[23]	AM1.5G	1.108V	30.0mA/cm^2	86.5%	28.7%
B.M. Kayes et al.[24]	ASTMG-173-03 global	1.107V	29.6mA/cm^2	84.1%	27.6%
M.A Green et al.[25]	ASTMG-173-03 global	1.122V	29.68mA/cm^2	86.5%	28.8%
Tomah Sogabe et al.[26]	AM1.5	1.0V	13mA/cm^2	83.5%	22.8%
Xutao Yu. Et al.[27]	AM1.5	1.16V	23.0mA/cm^2	77.7%	20.2%
Kevin L.Schulte et al.[28]	AM1.5G	1.09V	29.01mA/cm^2	85.33%	27%
Valentin Daniel et al.[29]	AM1.5G	1.012 $\pm$ 0.014V	26.28 $\pm$ 0.58mA/cm^2	81.98 $\pm$ 2.58 %	21.8 $\pm$ 0.78%
Laila S. Mattos et al.[30]	AM1.5G	1.077V	2.22mA	84.0%	23.5%
Our model	AM1.5G	1.312V	31.36mA/cm^2	83.31%	34.38%

5. Conclusion

A five-layer gallium arsenide solar cell was studied and simulated using the One-Dimensional Solar Cell Capacitance Simulator. Its depth analysis was studied at a thickness of 0.8µm of GaAs emitter layer and 2.0µm of GaAs base layer. The optimum efficiency depends on the doping concentrations and layer thickness. Also, the integration of an AlGaAs window layer at the top contributes to the device's performance

.

The analysis results in an impressive efficiency of 34.38%. In the present work, numerical solutions indicate that increasing thickness improves the performance and demonstrates a maximum efficiency at a band gap of 1.42eV. The observed characteristics show alignment with the previous research papers on Gallium arsenide solar cells. The modulation due to the concentration and thickness demonstrates that the structure is more sensitive towards the emitter layer—additionally, the study inspects the temperature effect on the structure. The suggested solar structure provides a low fill factor of 83.31%, a high current density of 31.36mA/cm^{2,} and a no-load voltage of 1.31V. Hence, alternative material combinations of the solar structure improves spectral response, reduce losses, and enhance efficiency.

References

[1] Kevin Gurbani Beepat et al., "Simulation of Multijunction Solar Cell Interfaces for Enhancement of the Power Conversion Efficiency," *Discover Applied Sciences*, vol. 6, pp. 1-19, 2024. [CrossRef] [Google Scholar] [Publisher Link]

[2] Gangasagar Sharma Gaudel et al., "Reflectance Minimization of GaAs Solar Cell with Single- and Double-Layer Anti-Reflection Coatings: A Simulation Study," *Coatings*, vol. 15, no. 2, pp. 1-13, 2025. [CrossRef] [Google Scholar] [Publisher Link]

[3] Chae-Won Kim et al., "Efficiency Enhancement of GaAs Single-Junction Solar Cell by Nanotextured Window Layer," *Applied Sciences*, vol. 12, no. 2, pp. 1-8, 2022. [CrossRef] [Google Scholar] [Publisher Link]

[4] Farzaneh Shahnooshi, and Ali A. Orouji, "Efficiency Improvement of Graphene/AlGaAs/GaAs Schottky Junction Solar Cells by Minimizing Optical Losses Through Front and Rear Surface Texturing," *Scientific Reports*, vol. 15, pp. 1-13, 2025. [CrossRef] [Google Scholar] [Publisher Link]

[5] Yanyan Wang et al., "Enhanced Antireflection and Absorption in Thin Film GaAs Solar Cells using Dielectric Composite Nanostructures," *Heliyon*, vol. 10, no. 23, pp. 1-7, 2024. [CrossRef] [Google Scholar] [Publisher Link]

[6] Ishika Das et al., "Wafer-Scale Correlated Morphology and Optoelectronic Properties in GaAs/AlGaAs Core-Shell Nanowires," *APL Materials*, vol. 13, no. 6, pp. 1-8, 2025. [CrossRef] [Google Scholar] [Publisher Link]

[7] Mohammad Nur-E-Alam et al., "Enhancing GAAS Solar Cell Efficiency through Nanostructured Features: A Comprehensive Review of Recent Advances, Challenges and Future Outlook," *Inorganic Chemistry Communications*, vol. 178, no. 1, pp. 1-16, 2025. [CrossRef] [Google Scholar] [Publisher Link]

[8] Antonio Luque, and Steven Hegedus, *Handbook of Photovoltaic Science and Engineering*, 2nd ed., Wiley, pp. 2011. [CrossRef] [Google Scholar] [Publisher Link]

[9] M.A. Green, *Solar Cells: Operating Principles, Technology, and System Applications*, Prentice Hall, 1981. [Google Scholar] [Publisher Link]

[10] S.M. Sze, and Kwok K. Ng, *Physics of Semiconductor Devices*, 3rd ed., Wiley, 2007. [CrossRef] [Google Scholar] [Publisher Link]

[11] Peter Würfel, and Uli Würfel, *Physics of Solar Cells: From Basic Principles to Advanced Concepts*, 3rd ed., Wiley, 2016. [Google Scholar] [Publisher Link]

[12] Donald A. Neamen, *Semiconductor Physics and Devices*, 4th ed., McGraw-Hill, pp. 1-8, 2011. [Google Scholar] [Publisher Link]

[13] Gerald B. Stringfellow, *Organometallic Vapor-Phase Epitaxy*, 2nd ed., Academic Press, 1999. [Google Scholar] [Publisher Link]

[14] Jenny Nelson, *The Physics of Solar Cells*, Imperial College Press, 2003. [CrossRef] [Google Scholar] [Publisher Link]

[15] R. People, and J.C. Bean, "Calculation of Critical Layer Thickness Versus Lattice Mismatch for Ge_xSi_{1-x}/Si Strained-Layer Heterostructures," *Applied Physics Letters*, vol. 47, no. 3, pp. 322-324, 1985. [CrossRef] [Google Scholar] [Publisher Link]

[16] H. Angus MacLeod, and H. Angus Macleod, *Thin-Film Optical Filters*, 4th ed., CRC Press, pp. 1-800, 2010. [CrossRef] [Google Scholar] [Publisher Link]

[17] Marc Burgelman et al., "SCAPS Manual," *University of Gent Department of Electronics and Information Systems*, pp. 1-159, 2016. [Google Scholar] [Publisher Link]

[18] Shizhao Fan et al., "16.8%-Efficient n^+/p GaAs Solar Cells on Si with High Short-Circuit Current Density," *IEEE Journal of Photovoltaics*, vol. 9, no. 3, pp. 660-665, 2019. [CrossRef] [Google Scholar] [Publisher Link]

[19] Daehwan Jung et al., "Low Threading Dislocation Density GaAs Growth on on-axis GaP/Si (001)," *Journal of Applied Physics*, vol. 122, no. 22, 2017. [CrossRef] [Google Scholar] [Publisher Link]

[20] Duy Phong Pham, Sunhwa Lee, and Junsin Yi, "Optimisation of Four-Terminal GaAs//Si Tandem Solar Cells Using Numerical Simulation," *Materials Science in Semiconductor Processing*, vol. 139, 2022. [CrossRef] [Google Scholar] [Publisher Link]

[21] R.C. Knechtli, R.Y. Loo, and G.S. Kamath, "High-Efficiency GaAs Solar Cells," *IEEE Transactions On Electron Devices*, vol. 31, no. 5, pp. 577-588, 1984. [CrossRef] [Google Scholar] [Publisher Link]

[22] Zekun Ren et al., "The GaAs/GaAs/Si Solar Cell – Towards Current Matching in an Integrated Two Terminal Tandem," *Solar Energy Materials & Solar Cells*, vol. 160, pp. 94-100, 2017. [CrossRef] [Google Scholar] [Publisher Link]

[23] Sun-Tae Hwang et al., "Bandgap Grading and $Al_{0.3}Ga_{0.7}As$ Heterojunction Emitter for Highly Efficient GaAs-based Solar Cells," *Solar Energy Materials and Solar Cells*, vol. 155, pp. 264-272, 2016. [CrossRef] [Google Scholar] [Publisher Link]

[24] Brendan M. Kayes et al., "27.6% Conversion Efficiency, A New Record for Single-Junction Solar Cells under 1 Sun Illumination," *2011 37th IEEE Photovoltaic Specialists Conference*, Seattle, WA, USA, 2011. [CrossRef] [Google Scholar] [Publisher Link]

[25] Martin A. Green et al., "Solar Cell Efficiency Tables (version 47)," *Progress in Photovoltaics*, vol. 14, no. 1, pp. 45-51, 2006. [CrossRef] [Google Scholar] [Publisher Link]

[26] Tomah Sogabe et al., "High-Efficiency InAs/GaAs Quantum Dot Intermediate Band Solar Cell Achieved Through Current Constraint Engineering," *Next Materials*, vol. 1, no. 2, pp. 1-11, 2023. [CrossRef] [Google Scholar] [Publisher Link]

[27] Xutao Yu, et al., "High Efficient Solar Cell Based on Heterostructure Constructed by Graphene and GaAs Quantum Wells," *Advanced Science*, vol. 10, no. 2, pp. 1-8, 2023. [CrossRef] [Google Scholar] [Publisher Link]

[28] Kevin L. Schulte et al., "Modeling and Design of III-V Heterojunction Solar Cells for Enhanced Performance," *Cell Reports Physical Science*, vol. 4, no. 9, pp. 1-15, 2023. [CrossRef] [Google Scholar] [Publisher Link]

[29] Valentin Daniel et al., "High-Efficiency GaAs Solar Cells Grown on Porous Germanium Substrate with Peeler Technology," *Solar RRL*, vol. 8, no. 1, pp. 1-15, 2024. [CrossRef] [Google Scholar] [Publisher Link]

[30] Laila S. Mattos et al., "New Module Efficiency Record: 23.5% Under 1-sun Illumination using Thin-Film Single-Junction GaAs Solar Cells," *2012 38th IEEE Photovoltaic Specialists Conference*, Austin, TX, USA, pp. 3187-3190, 2012. [CrossRef] [Google Scholar] [Publisher Link]